PIER C

(Received 15 November 2025, Accepted 11 December 2025, Scheduled 16 January 2026)

Wide-Angle Scanning Phased Array Based on Phase Mode Antenna Element

Ming-Qi Yi and Shen-Yun Wang*

Research Center of Applied Electromagnetics
Nanjing University of Information Science and Technology, Nanjing 210044, China

ABSTRACT: To address the significant gain degradation that conventional phased arrays suffer during wide-angle scanning, a linear antenna array based on phase-mode antenna elements was proposed. The phase-mode antenna element has a three-layer structure with two feeding ports. It can operate in odd, even, and hybrid modes by using different excitation strategies, and continuous beam scanning is achieved using the hybrid mode, which results in a wide-angle beam scanning performance of the antenna array. The maximum beam gain can be obtained using the method of maximum power transmission efficiency (MMPTE) compared with the traditional beam scanning method. The optimal excitation distributions calculated by the MMPTE lead to a significant improvement in the wide-angle beam scanning for the phase-mode antenna array.

1. INTRODUCTION

Phased arrays have been widely used in radar and communication systems for non-inertial beam scanning, high-gain beams, convenient beam control, and robust interference rejection [1]. According to phased-array theory, the beam gain decreases with the scanning angle as the effective aperture decreases with the scanning angle, as well as the mutual coupling between the elements and the limitation of the beamwidth of the element pattern [2]. This disadvantage limits its application in radar and wireless communications. Hence, to broaden the beam coverage, a wide-angle scanning phased-array antenna is essential [3].

Many techniques have been proposed to realize the wide-angle beam scanning of antenna arrays. These approaches are mainly categorized into three categories. First, a common approach is to employ a tightly coupled array that can enlarge the beam scanning range and realize an ultra-wide bandwidth by imitating the continuous current [4–10]. However, there are still some limitations for tightly coupled arrays, such as high profile, complex integrated balun, high fabrication accuracy, and high cost. Another way to increase the beam scanning range of the phased arrays is to use pattern reconfigurable elements, whose characteristics can be changed by redistributing the current flow in the radiating patch of the antenna.

One type of pattern-reconfigurable element is to load a parasitic structure onto the antenna element. To change the current flow and redistribute it in a radiating patch, active switches are usually required, such as radio frequency (RF) switches, pin diodes, and varactor diodes. However, these active switches require a biasing network, resulting in a complex structure that affects the radiation performance of the antenna array [11–16].

Another type of pattern-reconfigurable element is phase-mode antenna element [17–20]. To reconfigure the radiation pattern, the phase difference between the dual ports of the phase-mode antenna element is introduced to change the transmission direction of the surface currents, which leads to different operating modes, including the odd, even, and hybrid modes. Consequently, the main beam direction can be flexibly controlled using wide-angle scanning characteristics. However, conventional implementations of such schemes often treat the phase difference between the dual ports of an element as a fixed value rather than a parameter available for optimization. Hence, the advantages of the phase mode array in maximizing the beam scanning performance have not been extensively explored.

In this paper, a 1-D wide-angle scanning phased array is proposed based on the phase-mode antenna element. The phase-mode antenna element can operate in odd, even, and hybrid modes by applying different excitation strategies. To obtain the maximum gain of the beam scanning at an arbitrary angle, the optimal excitation distribution (OED) was calculated using the extended method of maximum power transmission efficiency (EMMPTE) [21]. The novelty of this study lies in the maximum gain value of the scanning beam by optimizing the excitation phase difference and power ratio for all phase-mode antenna elements.

2. WIDE-ANGLE SCANNING ANTENNA DESIGN

2.1. Phase Mode Antenna Element Structure

The geometry of the phase-mode antenna element is shown in Fig. 1. It consists of a continuous metal ground, a rectangular patch over the ground plane, and a metasurface integrated on the topside. The 3D and top views of the rectangular patch

* Corresponding author: Shen-Yun Wang (wangsy2006@126.com).

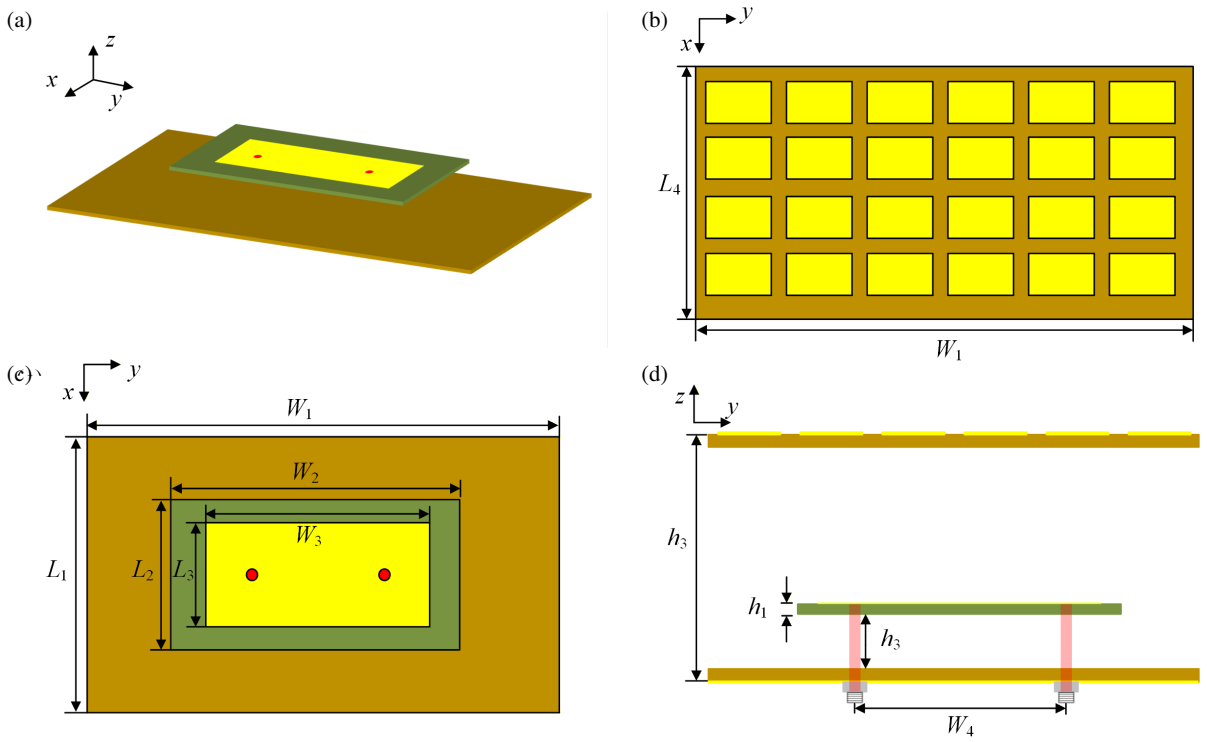

FIGURE 1. Configuration of the proposed antenna element. (a) 3D view of the rectangular patch integrated over the ground plane. (b) Geometry of the metasurface. (c) Top view of the rectangular patch integrated over the ground plane. (d) Side view of the phase-mode antenna element.

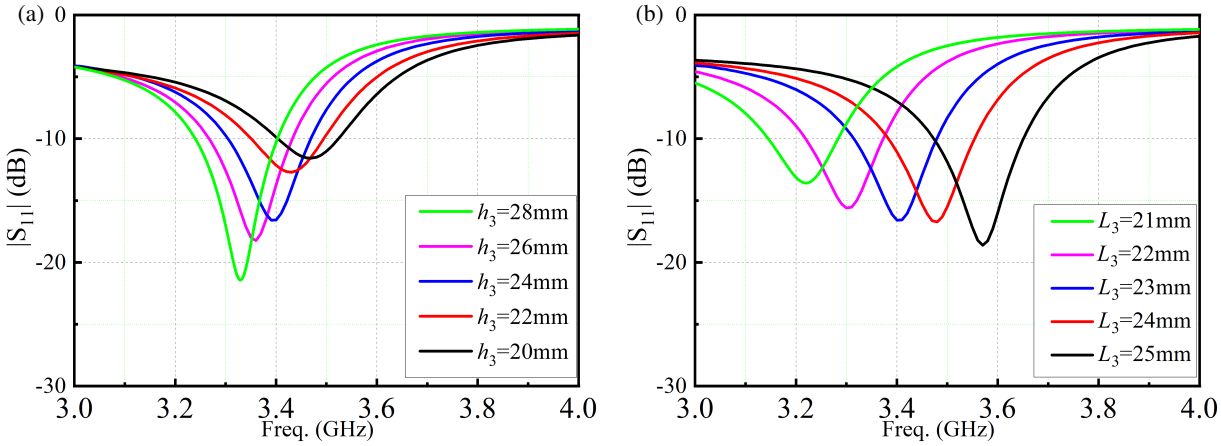

FIGURE 2. Simulated $|S_{11}|$ of the proposed antenna element for different (a) metasurface height h_3, (b) patch width L_3.

designed on an FR-4 substrate and integrated over the ground plane are shown in Figs. 1(a) and (c), respectively. Dual symmetrical ports were designed to feed the rectangular patch using two coaxial probes that passed through the ground plane. The metasurface is composed of 4×6 rectangular patches on another FR-4 substrate, as shown in Fig. 1(b), which was designed to achieve wide-angle impedance matching for the rectangular radiation patch. A side view of the phase-mode antenna element is shown in Fig. 1(d).

To understand the operating principle and optimize the antenna performance, a parametric study was conducted on several key geometric parameters. The effect of metasurface height h_3 on the reflection coefficient of the antenna is shown in Fig. 2(a). It was found that the resonant frequency shifted towards lower frequencies when the metasurface height increased from 20 to 28 mm. Next, the reflection coefficient of the antenna element versus the patch width L_3 is simulated, as shown in Fig. 2(b). It can be observed that the resonant frequency shifts to lower frequencies with an increase in patch width. Based on the comprehensive parametric study, the final optimized dimensions for the proposed antenna element were determined for working at 3.4 GHz. The parameters used are listed in Table 1.

2.2. Working Principle of the Element

The pattern reconfigurability of the proposed antenna element was based on the principle of mode superposition. The ampli-

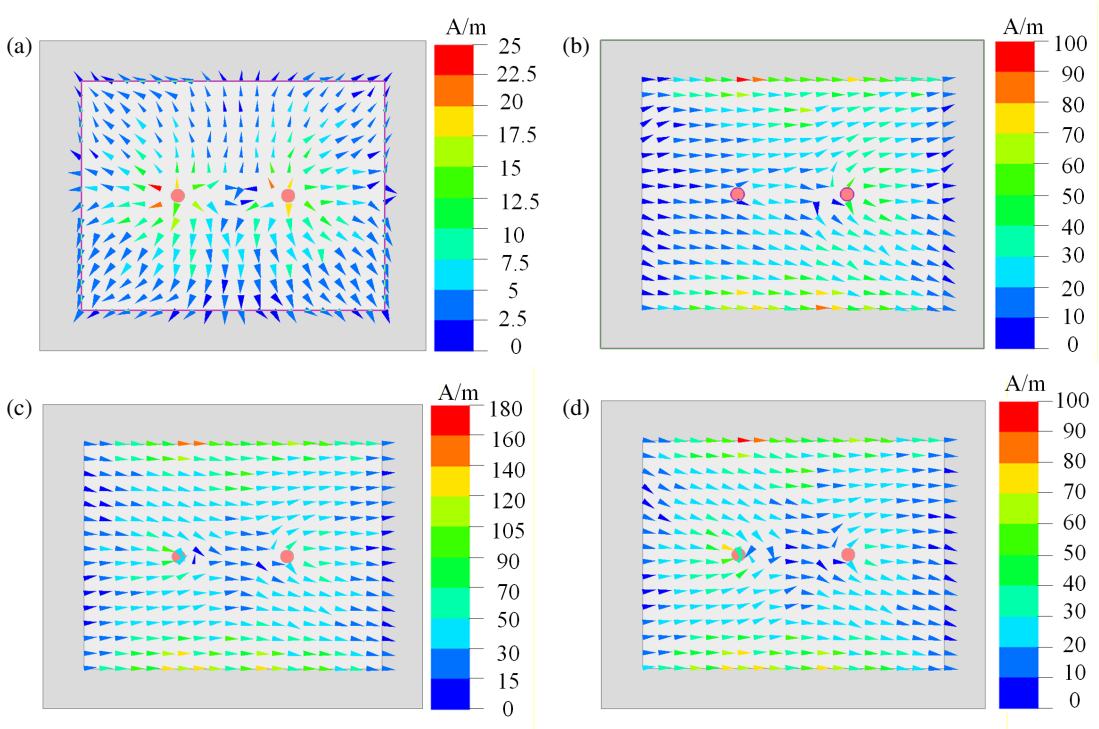

FIGURE 3. Surface current distributions of diverse modes with phase difference at (a) $\Delta\varphi = 0^\circ$ (even mode), (b) $\Delta\varphi = 90^\circ$ (mixed mode), (c) $\Delta\varphi = 180^\circ$ (odd mode), and (d) $\Delta\varphi = 270^\circ$ (mixed mode).

TABLE 1. Geometrical parameters of the antenna element.

Name	Value(mm)	Name	Value(mm)
W_1	90	L_2	29
W_2	38	L_3	23
W_3	32	L_4	25
W_4	10	h_2	3
L_1	40	h_3	24
h_1	1		

tudes of the signals at oorts 1 and 2 are denoted by A_1 and A_2, respectively. The phases of the signals at ports 1 and 2 are denoted by φ_1 and φ_2. Therefore, the phase difference is defined as $\Delta\varphi = \varphi_1 - \varphi_2$ which can be continuously controlled over the range of $[\pi-, \pi]$.

The antenna can operate in two fundamental radiation modes: even and odd. An even mode is generated when the two ports are excited with $\Delta\varphi = 0$; an odd mode is produced when the dual ports are excited with $\Delta\varphi = \pm\pi$; hybrid mode is defined if the dual ports are excited with other phase difference. The hybrid mode can be treated as a combination of the fundamental even and odd modes. By continuously changing $\Delta\varphi$, the contributions of these two modes to the hybrid mode can be adjusted. Consequently, radiation patterns can be reconfigured.

The radiation pattern of each mode is determined by the surface current distribution on the antenna element. Diverse surface current distributions can be obtained by feeding the two ports with different $\Delta\varphi$, as shown in Figures 3(a)–(d). The resultant radiation patterns are shown in Figures 4(a)–(d).

When the $\Delta\varphi$ was set to 0°, a symmetrical surface current distribution with respect to the center of the two ports is obtained, as shown in Figure 3(a). Consequently, the radiation pattern splits in the normal direction, as shown in Figure 4(a). When the $\Delta\varphi$ was set 180°, a surface current distribution with the same direction and balanced strength on the left and right sides is obtained, as shown in Figure 3(c). Consequently, a normal radiation pattern is generated, as shown in Figure 4(c). When the $\Delta\varphi$ is set 90° (270°), a surface current distribution in the same direction but a stronger surface current on the right (left) side is obtained, as shown in Figure 3(b) (Figure 3(d)). In this case, a radiation pattern pointing to the right (left) side was obtained, as shown in Figure 4(b) (Figure 4(d)).

In summary, the proposed dual-port antenna element achieved continuous beam scanning by simply adjusting the phase difference between the two ports. This capability is pivotal for enhancing the wide-angle beam scanning performance of phased arrays.

3. WIDE-ANGLE SCANNING ARRAY

3.1. Structure of the Antenna Array

Based on the designed antenna element, a 1×4 linear antenna array was designed and fabricated, and the feeding ports were denoted as Port-1 to Port-8, as shown in Figure 5. It consists of three layers: the top layer is the metasurface; the middle layer is fabricated with rectangular patches; and the bottom layer is metal ground. The top and middle layers were supported by nylon columns on the ground layer. The antenna array has transverse dimensions of $360 \times 40\,\text{mm}^2$ ($4.41\lambda_0 \times 0.46\lambda_0$),

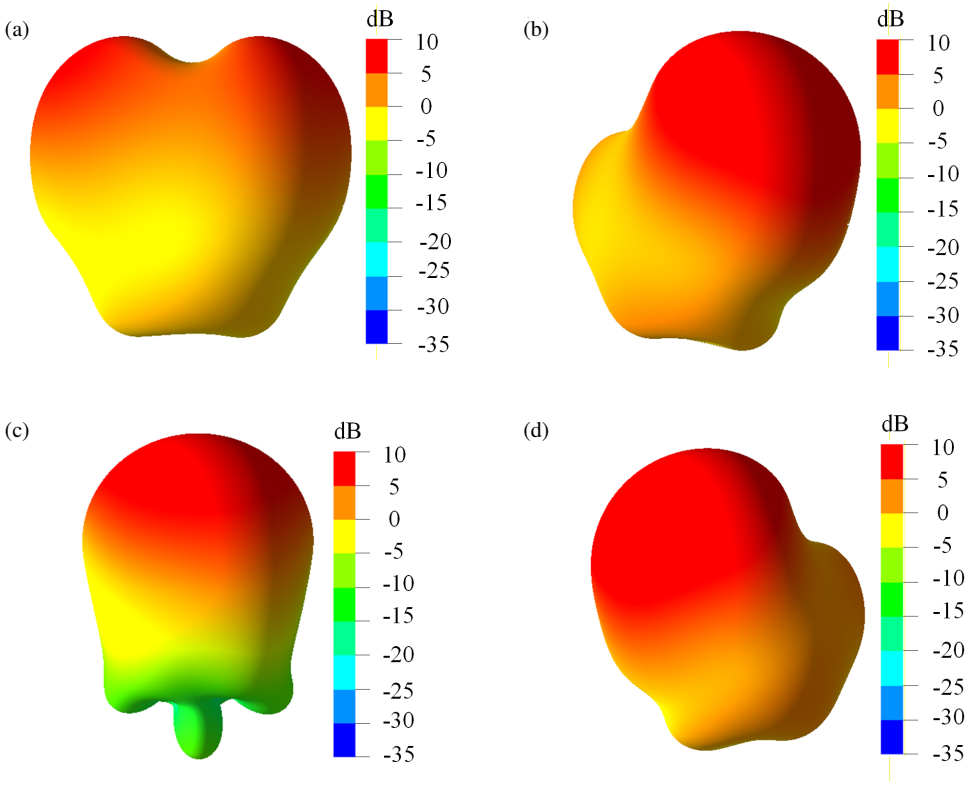

FIGURE 4. Simulated radiation patterns of diverse modes with phase difference at (a) $\Delta\varphi = 0^\circ$ (even mode), (b) $\Delta\varphi = 90^\circ$ (mixed mode), (c) $\Delta\varphi = 180^\circ$ (odd mode), and (d) $\Delta\varphi = 270^\circ$ (mixed mode).

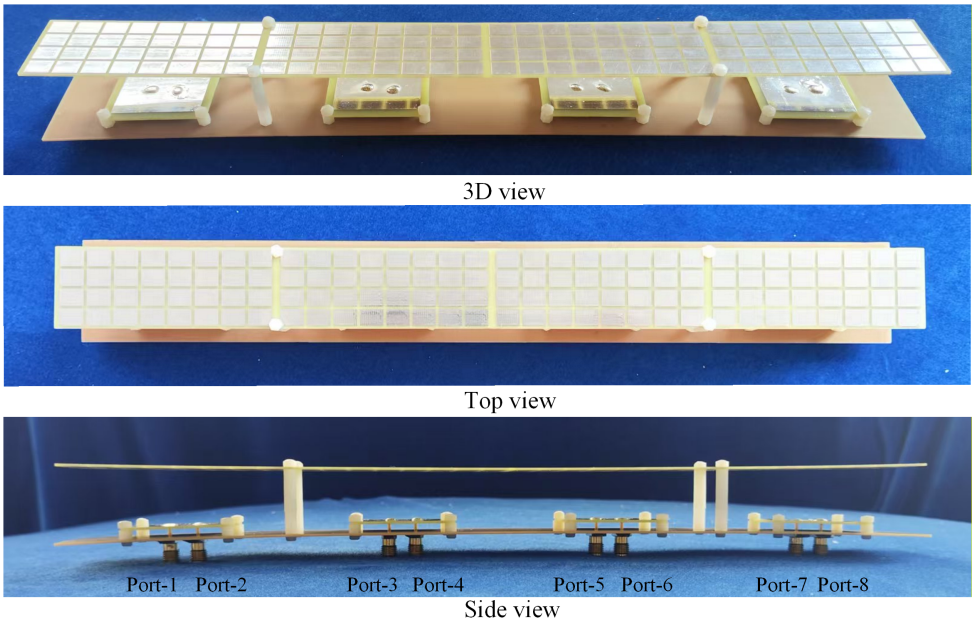

FIGURE 5. Configuration of the multilayer antenna array.

but the top metasurface layer has dimensions of $360 \times 30\,\text{mm}^2$ ($4.41\lambda_0 \times 0.34\lambda_0$).

The measured and simulated active $|S_{11}|$ and $|S_{55}|$ of the antenna array are plotted in Figures 6(a) and (b), respectively. It can be seen that good impedance matching is achieved at 3.4 GHz for different beam scanning angles.

3.2. Beam Scanning Method

A scanning beam in the desired direction can be realized by controlling the excitation distribution of the antenna array. Traditional beam scanning methods are usually based on the array factor, and they fail when the array factor is not available, such as in the case of different element patterns, complicated mount-

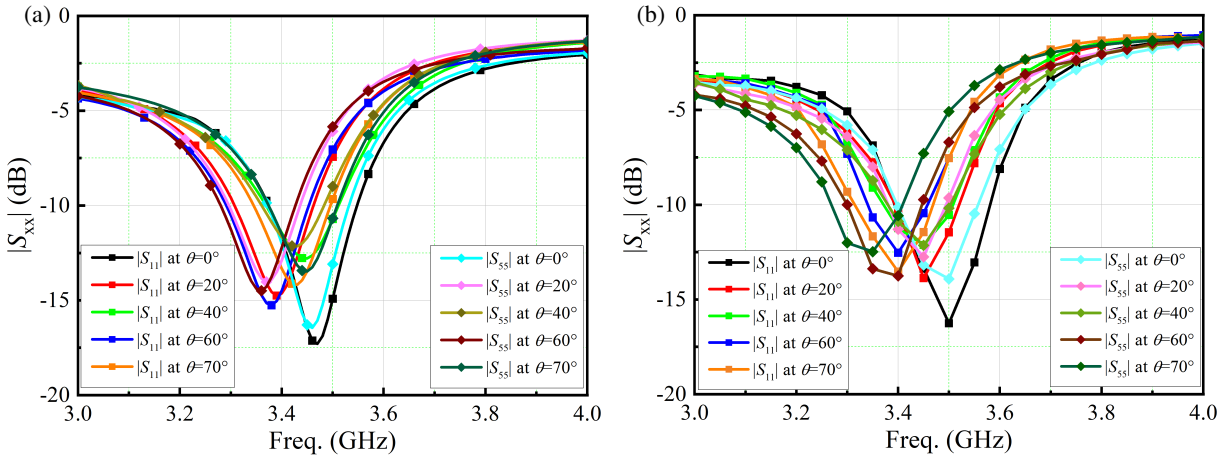

FIGURE 6. (a) Simulated active $|S_{11}|$ and $|S_{55}|$, and (b) measured active $|S_{11}|$ and $|S_{55}|$.

ing platforms of the antenna array, and mutual coupling among the elements. In this study, the EMMPTE is used to optimize the excitation amplitudes and phases of the array elements, ensuring the maximum possible gain value of the scanning beam in the desired direction.

As illustrated in Figure 7, a generalized wireless power transmission (GWPT) system is set up between the antenna array and terminal spot $P(r_p, \theta)$, which has a mapping position $P'(r_0, \theta)$ on a far-field arc with respect to the phase center of the antenna array.

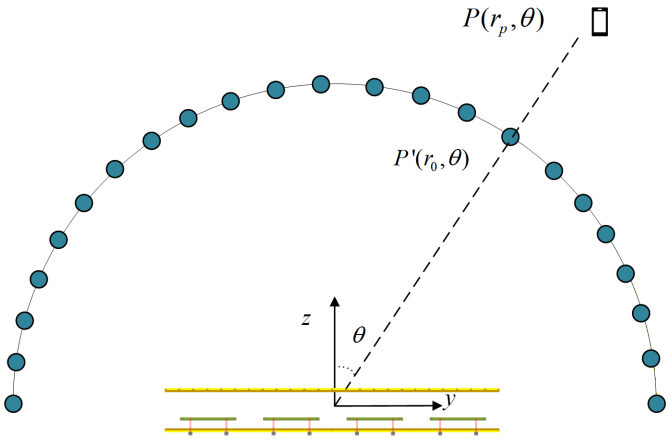

FIGURE 7. Generalized wireless power transmission system.

Next, a new performance index is introduced, which is defined as the ratio of the electric-field energy density at the mapping spot to the total input power of the deformed array:

$$\eta = \frac{\frac{\varepsilon_0}{2}\left|E\left(P'\right)\right|^2}{P_{in}} \tag{1}$$

where the numerator is the total electric field energy density at the mapping spot, and the dominator represents the total input power of the antenna array. The beam can be directed towards the terminal by maximizing the η, which guarantees the maximum possible gain value of the beam. Assuming that all transmitting antenna elements are well matched, the total electric field at the mapping position can be expressed as:

$$E\left(r_p\right) = \sum_{j=1}^{N} a_j E_j\left(r_p\right) \tag{2}$$

where N is the number of antenna elements; $E_j(r_p)$ is the electrical field generated by the j-th transmitting antenna element at the mapping position when it is excited by $a_j = 1$, and the other elements are terminated in their own characteristic impedances. Hence, the total electric fields at the mapping position can be written as

$$E\left(P'\right) = [E_{rt}][a] \tag{3}$$

where

$$[E_{rt}] = \left[E_1\left(P'\right), E_2\left(P'\right), \ldots, E_3\left(P'\right)\right],$$

$$[a] = \left[a_1, a_2, \ldots, a_N\right]^T,$$

Using (2) and (3), the performance index (1) can be written as

$$\eta = \frac{\frac{\varepsilon_0}{2}\left|[E_{rt}][a]\right|^2}{\frac{1}{2}\left|[a]\right|^2} = \frac{\langle [A][a], [a]\rangle}{\langle [a], [a]\rangle} \tag{4}$$

where $[A] = \varepsilon_0[\bar{E}_{rt}]^T[E_{rt}]$ and $P_{in} = |[a]|^2/2$. The *PTE* was determined using the excitation distribution $[a]$. By maximizing (4), the eigenvalue equation is obtained as

$$[A][a] = \eta \cdot [a]. \tag{5}$$

This equation can be solved using QR methods, which are used to find the solution of the eigenvalues by factorizing the matrix into an orthogonal matrix $[Q]$ and an upper triangular matrix $[R]$. The maximum eigenvalue represents the maximum performance index η, and the corresponding eigenvector $[a]$ is the ODE.

It should be mentioned that the electric fields $[E_{rt}]$ can be extracted in advance through simulation or measurement, and the ODEs can be calculated in real-time by solving (5) once the desired direction is confirmed.

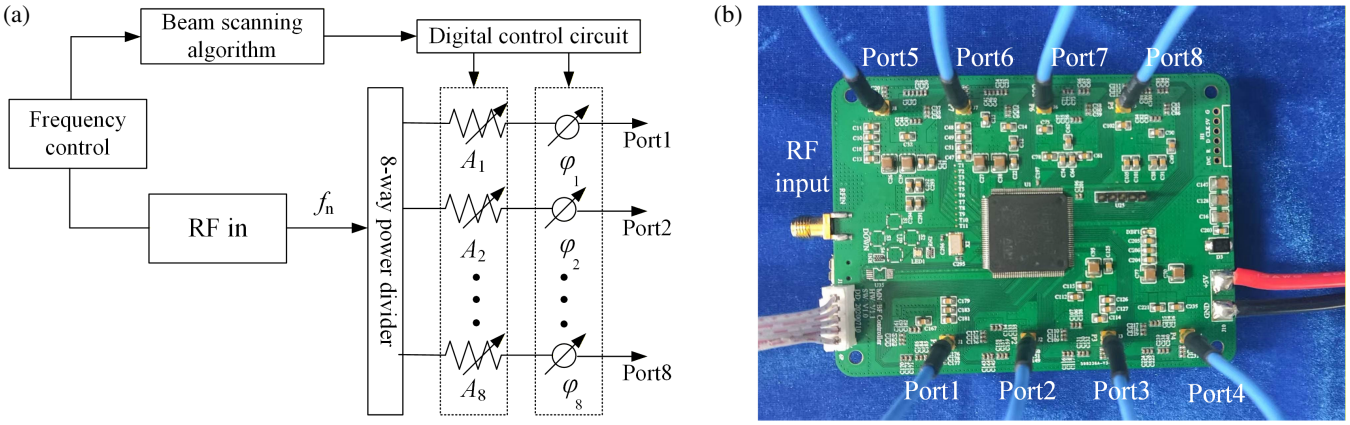

FIGURE 8. Digital-control feeding circuit: (a) Schematic; (b) Photo.

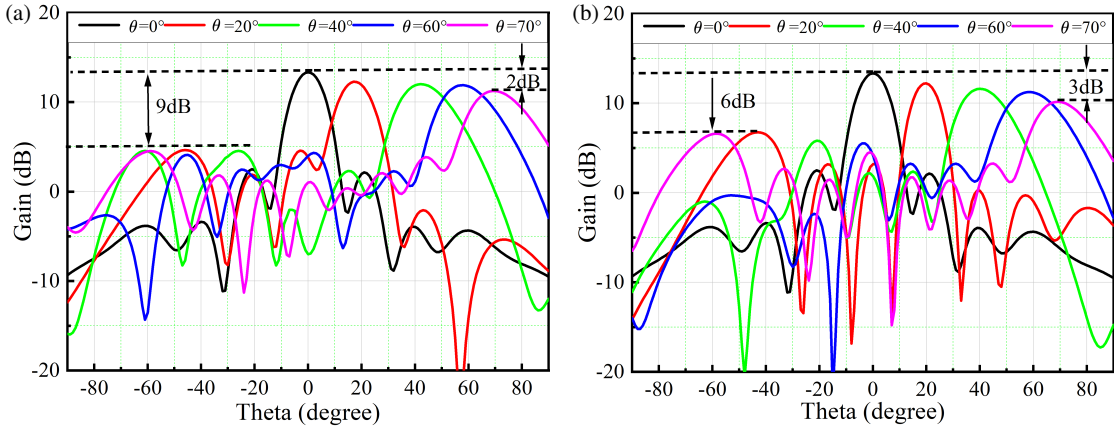

FIGURE 9. Simulated scanning beam patterns using (a) MMPTE, and (b) OFEDS at 3.4 GHz.

TABLE 2. OEDs of the antenna array for different beam directions.

Port	0°	20°	40°	60°	70°
1	$1\angle°$	$0.42\angle-112°$	$0.19\angle-12°$	$0.19\angle81°$	$0.3\angle149°$
2	$1\angle180°$	$0.41\angle23°$	$0.38\angle104°$	$0.2\angle170°$	$0.28\angle130°$
3	$1\angle0°$	$0.44\angle-20°$	$0.35\angle-175°$	$0.16\angle84°$	$0.25\angle115°$
4	$1\angle180°$	$0.28\angle132°$	$0.45\angle-61°$	$0.55\angle145°$	$0.26\angle89°$
5	$1\angle0°$	$0.25\angle94°$	$0.19\angle6°$	$0.25\angle-18°$	$0.3\angle68°$
6	$1\angle180°$	$0.31\angle-74°$	$0.36\angle180°$	$0.4\angle87°$	$0.28\angle40°$
7	$1\angle0°$	$0.29\angle-147°$	$0.23\angle-80°$	$0.16\angle-30°$	$0.27\angle24°$
8	$1\angle180°$	$0.34\angle0°$	$0.36\angle0°$	$0.56\angle0°$	$0.26\angle0°$

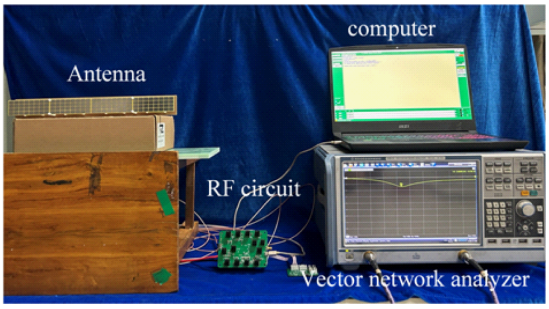

FIGURE 10. Setup of the antenna system.

TABLE 3. The adopted fixed excitation distribution.

Scanning Angle	0°	2°	40°	6°	70°
$\Delta\varphi$	180°	100°	70°	35°	20°
A_1/A_2	1	0.3	0.4	0.6	1

3.3. Digital-Control Feeding Circuit

To excite the antenna array with the ODE calculated using (5), a digital-control feeding circuit is designed, as shown in Figure 8. A schematic of the feeding circuit is illustrated in Figure 8(a), which consists of eight channels using an 8-way power

TABLE 4. OFEDs of the array for beam directions.

Port	0°	20°	40°	60°	70°
1	$1\angle 0°$	$0.3\angle -20°$	$0.4\angle 130°$	$0.6\angle -115°$	$1\angle 14°$
2	$1\angle 180°$	$1\angle -120°$	$1\angle 60°$	$1\angle -150°$	$1\angle 120°$
3	$1\angle 0°$	$0.3\angle 140°$	$0.4\angle 10°$	$0.6\angle 175°$	$1\angle 100°$
4	$1\angle 180°$	$1\angle 40°$	$1\angle -80°$	$1\angle 140°$	$1\angle 8°$
5	$1\angle 0°$	$0.3\angle -60°$	$0.4\angle -150°$	$0.6\angle 105°$	$1\angle 6°$
6	$1\angle 180°$	$1\angle -160°$	$1\angle 14°$	$1\angle 70°$	$1\angle 40°$
7	$1\angle 0°$	$0.3\angle 100°$	$0.4\angle 7°$	$0.6\angle 35°$	$1\angle 20°$
8	$1\angle 180°$	$1\angle 0°$	$1\angle 0°$	$1\angle 0°$	$1\angle 0°$

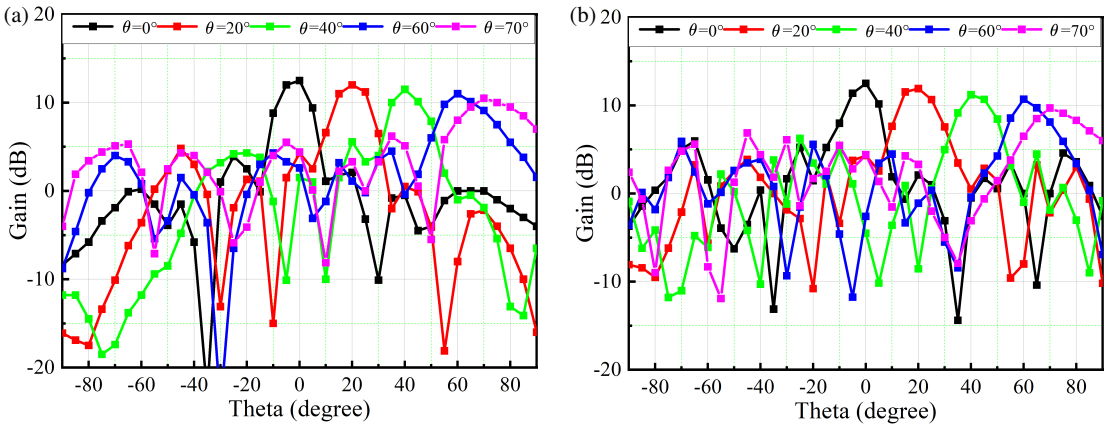

FIGURE 11. Measured scanning beam patterns using (a) MMPTE, and (b) OFEDS at 3.4 GHz.

divider. Each channel consists of a 6-bit phase shifter with a phase shifting resolution of $5.625°$ ($360°/2^6$) and a 6-bit attenuator with a maximum attenuation of 31.5 dB and 0.5 dB (31.5 dB/2^6) amplitude control resolution. A photograph of the fabricated digital-control feeding network is shown in Figure 8(b).

3.4. Beam Scanning Performance

To validate the wide-angle beam scanning performance of the proposed antenna array based on the phase-mode antenna element, beam patterns with different scanning angles were simulated using the EMMPTE, as shown in Figure 9(a). It was found that the beam gain is reduced by 2.0 dB at 70° compared with that at 0°, and the gain difference between the grating lobe and main beam is larger than 9 dB. The ODEs of the antenna array used to form the beam patterns were calculated using Eq. (5) and listed in Table 2. It was found that the excitation amplitude ratio A_1/A_2 and phase difference $\Delta\varphi$ of each antenna element were not identical for a specific beam scanning angle.

For comparison, beam patterns with the same scanning angles were simulated using the optimal fixed excitation distribution (OFED) of the phase-mode antenna element reported in [20], as shown in Figure 9(b). In this case, the $\Delta\varphi$ and A_1/A_2 are identical for all phase-mode antenna elements, and they have been optimized for different scanning angles, as listed in Table 3. The OFEDs of the antenna element for different array beam scanning angles are listed in Table 4. It is found that the beam gain is reduced by 3.0 dB at 70°, and the gain difference between the grating lobe and main beam is larger than 6.0 dB. It is obvious that the grating lobes are well suppressed when the beams scan at large angles using the EMMPTE. The beam gain also decreases slowly with the canning angle compared with the results obtained using the method reported in [20].

Finally, the antenna system was set up with the fabricated antenna array, feeding circuit, and connecting cables, where the OED was calculated on a laptop computer and transferred to the feeding circuit via a USB cable, as shown in Figure 10. Next, the beam patterns excited with the ODEs and OFEDs are measured in an anechoic microwave chamber, as shown in Figures 11(a) and (b), respectively. It can be seen that the measured results agree well with the simulation ones. The measured realized gain is 12.5 dBi, 12.1 dBi, 11.4 dBi, 11 dBi, and 10.3 dBi, respectively, when the beam scans at 0°, 20°, 40°, 60°, and 70° by using MMPTE. The measured realized gain is 12.5 dBi, 12 dBi, 11.2 dBi, 10.7 dBi, and 9.7 dBi, respectively, when the beam scans at 0°, 20°, 40°, 60°, and 70° excited with OFEDs. In addition, the antenna efficiency was evaluated using the measured realized gain and simulated directivity, which is given G_{realized}/D. As a result, the antenna efficiency varies from 84% to 89% when the beam scans from 0° to 70° using both excitation methods. In other words, the antenna efficiency remains stable for different beam scanning angles and excitation methods.

4. CONCLUSIONS

In this paper, a linear wide-angle scanning phased array is proposed based on a phase-mode antenna element. The phase-mode antenna element can operate in odd, even, and hybrid modes by using different excitation strategies, which makes the proposed antenna element achieve continuous beam scanning characteristics. Consequently, grating-lobe suppression and wide-angle scanning ranges were achieved for the proposed phased array. The maximum gain value of the scanning beam was obtained using EMMPTE. Such an excitation strategy improves the wide-angle beam scanning performance of the phase-mode antenna array. Meanwhile, it has a positive effect on the improvement of current wireless communication systems and radar systems.

ACKNOWLEDGEMENT

This research was funded by the National Natural Science Foundation of China under Grant No. 62301262.

REFERENCES

[1] Yaseen, N. W. and J. R. Mohammed, "Scanned antenna arrays with random deactivated elements," *Progress In Electromagnetics Research Letters*, Vol. 119, 1–6, 2024.

[2] Bai, Y.-Y., S. Xiao, M.-C. Tang, Z.-F. Ding, and B.-Z. Wang, "Wide-angle scanning phased array with pattern reconfigurable elements," *IEEE Transactions on Antennas and Propagation*, Vol. 59, No. 11, 4071–4076, 2011.

[3] Yang, G., J. Li, R. Xu, Y. Ma, and Y. Qi, "Improving the performance of wide-angle scanning array antenna with a high-impedance periodic structure," *IEEE Antennas and Wireless Propagation Letters*, Vol. 15, 1819–1822, 2016.

[4] Doane, J. P., K. Sertel, and J. L. Volakis, "A wideband, wide scanning tightly coupled dipole array with integrated balun (TCDA-IB)," *IEEE Transactions on Antennas and Propagation*, Vol. 61, No. 9, 4538–4548, 2013.

[5] Yetisir, E., N. Ghalichechian, and J. L. Volakis, "Ultrawideband array with 70° scanning using FSS superstrate," *IEEE Transactions on Antennas and Propagation*, Vol. 64, No. 10, 4256–4265, 2016.

[6] Kim, S. and S. Nam, "Ultra-wideband and wide-angle insensitive absorber based on TCDA-under-tightly coupled dipole array," *IEEE Transactions on Antennas and Propagation*, Vol. 69, No. 9, 5682–5690, 2021.

[7] Zhao, L., H. Zhu, Y. Di, H. Zhao, J. Mou, and C. Hu, "Design of joinable antenna array with wide-angle scanning," *IEEE Antennas and Wireless Propagation Letters*, Vol. 24, No. 2, 479–483, 2025.

[8] Zhao, L., H. Zhu, C. Ding, G. Liu, H. Zhao, J. Mou, and Y. J. Guo, "An ultrawideband dual-polarized tightly coupled dipole array (TCDA) with wide scanning range," *IEEE Antennas and Wireless Propagation Letters*, Vol. 23, No. 7, 1961–1965, 2024.

[9] Hu, C.-H., B.-Z. Wang, G.-F. Gao, R. Wang, S.-Q. Xiao, and X. Ding, "Conjugate impedance matching method for wideband and wide-angle impedance matching layer with 70° scanning in the H-plane," *IEEE Antennas and Wireless Propagation Letters*, Vol. 20, No. 1, 63–67, 2021.

[10] Yu, D., Z.-C. Hao, L. Sun, K. Yan, W. Zhang, and Y. Jiang, "Design of a wideband wide scanning phased antenna array with FSS superstrates," *Progress In Electromagnetics Research Letters*, Vol. 112, 41–47, 2023.

[11] Zhang, Y., S. Tang, J. Rao, C.-Y. Chiu, X. Chen, and R. Murch, "A dual-port dual-beam pattern-reconfigurable antenna with independent 2-D beam-scanning," *IEEE Transactions on Antennas and Propagation*, Vol. 72, No. 10, 7628–7643, 2024.

[12] Du, Y., Y.-H. Yang, Z.-B. Han, J.-Y. Li, and S.-G. Zhou, "Wide-angle scanning array based on reconfigurable element integrated of binary array," *IEEE Antennas and Wireless Propagation Letters*, Vol. 23, No. 6, 1949–1953, 2024.

[13] Sun, B.-F., X. Ding, Y.-F. Cheng, and W. Shao, "2-D wide-angle scanning phased array with hybrid patch mode technique," *IEEE Antennas and Wireless Propagation Letters*, Vol. 19, No. 4, 700–704, 2020.

[14] Yang, G. and S. Zhang, "Dual-polarized wide-angle scanning phased array antenna for 5G communication systems," *IEEE Transactions on Antennas and Propagation*, Vol. 70, No. 9, 7427–7438, 2022.

[15] Dai, C. and L. Gan, "A dual-polarized wide-angle scanning antenna with high isolation for Van Atta applications," *Progress In Electromagnetics Research Letters*, Vol. 103, 81–88, 2022.

[16] Gao, G.-F., X. Ding, Y.-F. Cheng, and W. Shao, "Dual-polarized wide-angle scanning phased array based on mutimode patch elements," *IEEE Antennas and Wireless Propagation Letters*, Vol. 18, No. 3, 546–550, 2019.

[17] Chen, Z., Z. Song, H. Liu, X. Liu, J. Yu, and X. Chen, "A compact phase-controlled pattern-reconfigurable dielectric resonator antenna for passive wide-angle beam scanning," *IEEE Transactions on Antennas and Propagation*, Vol. 69, No. 5, 2981–2986, 2021.

[18] Wang, K., J. Geng, H. Zhou, S. Yang, R. Zhao, J. Chen, J. Lu, X. Tang, J. Zhang, and R. Jin, "A novel low-profile phased antenna with dual-port and its application in 1-D linear array to 2-D scanning," *IEEE Transactions on Antennas and Propagation*, Vol. 70, No. 8, 6718–6731, 2022.

[19] Wang, K., J. Geng, S. Yang, J. Lu, R. Zhao, X. Tang, X. Li, D. Su, A. Zhang, H. Li, E. Li, and R. Jin, "A novel phase mode antenna with triport and its application in a 1-D generalized phased array to 2-D scanning," *IEEE Transactions on Antennas and Propagation*, Vol. 71, No. 10, 8072–8087, 2023.

[20] Wang, Y., Q. Xue, Z. Hu, and S. Liao, "Mixed-modes-enabled element-level beamforming antenna with enhanced isolation for phased array applications," *IEEE Transactions on Antennas and Propagation*, Vol. 72, No. 5, 4577–4582, 2024.

[21] Geyi, W., "The method of maximum power transmission efficiency for the design of antenna arrays," *IEEE Open Journal of Antennas and Propagation*, Vol. 2, 412–430, 2021.